Solid Freeform Fabrication 2023: Proceedings of the 34th Annual International Solid Freeform Fabrication Symposium – An Additive Manufacturing Conference
Reviewed Paper

Effect of heat treatment on the microstructure and mechanical properties of Monel K500 alloy fabricated via L-PBF and LP-DED

Indrajit Nandi[1,2], Reza Ghiaasiaan[1,2], Nabeel Ahmad[1,2], Paul R. Gradl[3], Shuai Shao[1,2], Nima Shamsaei[1,2*]

[1] National Center for Additive Manufacturing Excellence (NCAME), Auburn University, Auburn, AL 36849, USA

[2] Department of Mechanical Engineering, Auburn University, Auburn, AL36849, USA

[3] NASA Marshall Space Flight Center, Propulsion Department, Huntsville, AL 35812, USA

*Corresponding author: shamsaei@auburn.edu

Phone: (334) 844-4839

Abstract

This study examines and compares the effect of different heat treatments (HT) on the microstructure and mechanical properties of Monel K500 fabricated using laser powder bed fusion (L-PBF) and laser powder directed energy deposition (LP-DED) technologies. The as-fabricated Monel K500 specimens exhibited dendritic microstructure and elemental micro-segregation due to high cooling rates induced during the fabrication process. The applicability of HT proposed in the literature for wrought Monel K500 was investigated for L-PBF and LP-DED using four different HT procedures involving hot isostatic pressing (HIP), solution annealing (SA), and aging. The mechanical properties of test specimens were evaluated using uniaxial tensile testing at room temperature. The microstructural evolution of test specimens during HT was analyzed using a scanning electron microscope. For all HT conditions investigated, L-PBF Monel K500 specimens consistently displayed higher strength and lower ductility compared to the LP-DED counterparts. The HT procedure involving HIP at 1160°C for 3hr at 100 MPa, SA at 1100°C for 15 min, and three step aging at 610°C for 16 hr, 540°C for 6 hr, and 480°C for 8 hr resulted in highest strength for both L-PBF and LP-DED fabricated Monel K500.

Keywords: Additive manufacturing; Monel K500; Ni-base superalloys; microstructure; tensile properties

Introduction

Monel K500 (UNS N05500) is a γ' precipitation hardened Ni-base superalloy and its major alloying element, copper (~30 wt.% Cu) provides solid solution strengthening and improved corrosion resistance [1–3]. This alloy is particularly attractive for its high strength and hardness, and find applications in offshore and marine industries [4,5]. Due to the high hardness, conventional manufacturing and machining of Monel K500 alloy are often costly [6,7].

Additive manufacturing (AM) can be an attractive alternative for fabricating net-shaped Monel K500 parts with little to no machining at reduced cost and time owing to its offered advantage of design flexibility and on-demand manufacturing [8,9]. Among different AM technologies, laser powder bed fusion (L-PBF) and laser powder directed energy deposition (LP-DED) are widely used [10]. Both processes fabricate parts in a layer-by-layer fashion with L-PBF process using scanning laser beams to selectively melt and fuse metal powder that is uniformly spread over a build plate and LP-DED process injecting metal powder into laser beam through a nozzle [11–13]. With AM being relatively new, the mechanical properties of additively manufactured Monel K500 parts have not been thoroughly investigated.

Due to the unique thermal characteristics of AM processes, such as rapid cooling and solidification, the AM microstructure in the non-heat treated (NHT) condition are different from the wrought counterparts and often varies among different AM processes due to their difference in thermal history [14–16]. Moreover, the presence of AM process-induced volumetric defects can be detrimental to the mechanical properties of

additively manufactured (AMed) parts [17]. This requires post-fabrication heat treatments (HT) to make the mechanical properties of AMed parts comparable to their wrought counterparts [18,19]. The existing HT procedures for the Monel K500 alloys are established for the wrought material and might not be optimum for L-PBF and LP-DED Monel K500. This motivates investigating the effect of different HT on the mechanical properties of L-PBF and LP-DED Monel K500. Four different HT procedures following the literature for the wrought Monel K500 alloy are designed and their effects on the tensile properties of L-PBF and LP-DED Monel K500 are evaluated to establish a favorable HT procedure for the L-PBF and LP-DED Monel K500.

Experimental procedures

The chemical compositions of the two powder batches used for the fabrication of L-PBF and LP-DED Monel K500 specimens are presented in Table 1. For L-PBF, vertical near net-shaped specimens of 10 mm gage diameter and 80 mm length were fabricated by Quadrus Corporation using a Concept Laser M2 L-PBF machine and for LP-DED, vertical cylindrical bars of 15 mm diameter and 100 mm length were fabricated by RPM Innovations Inc. using a 557 LP-DED machine. The process parameters are listed in Table 2.

Table 1. Chemical compositions of the two Monel K500 powder batches, used to fabricate the L-PBF and LP-DED Monel K500 specimens.

Process	Elements	Cu	Al	Fe	Mn	Ti	Si	C	O	Ni
L-PBF	wt.%	28.4	2.88	0.43	0.75	0.60	<0.005	0.10	0.016	Bal.
LP-DED	wt.%	30	2.71	0.2	0.1	0.72	0.02	0.01	0.01	Bal.

Table 2. Process parameters used to fabricate the L-PBF and LP-DED Monel K500 specimens.

Process	Power (W)	Travel speed (mm/s)	Spot size (mm)	Hatch spacing (mm)	Layer thickness (mm)	Powder feed rate (g/min)	Inert gas
L-PBF	152	600	0.120	0.105	0.030	---	Ar
LP-DED	1070	16.93	---	---	0.381	16.5	Ar

Post fabrication, four different HT procedures, as listed in Table 3, were applied to the L-PBF and LP-DED Monel K500 specimens. All specimens underwent hot isostatic pressing (HIP) at 1163°C for 3 hours at a pressure of 100 MPa and furnace cooled (FC) to room temperature, followed by solution annealing (SA) at 1100°C for 15 min, and argon quenched (AQ) to room temperature. Finally, the hot isostatic pressed and annealed specimens were divided into four different groups and subjected to single and multi-step aging cycle, as listed in Table 3.

Table 3. Thermal treatments applied for the Monel K500 specimens in this study, designated as HT1, HT2, HT3, and HT4.

Designations	HIP	SA	Aging: Step 1	Aging: Step 2	Aging: Step 3
HT1	1163°C/100MPa/3hr FC	1100°C/15min AQ	610°C/8hr AQ		
HT2			610°C/16hr AQ		
HT3			610°C/16hr FC	480°C/8hr AQ	
HT4			610°C/16hr FC	540°C/6hr FC	480°C/8hr AQ

Small coupons were excised from the NHT and heat treated Monel K500 specimens and microstructural characterizations were performed on the transverse plane, i.e., parallel to the build direction. The coupons were mounted on cold epoxy resin and the top surface were mirror polished to remove any surface scratches according to the ASTM-E3 standard [20]. A Zeiss Crossbeam 550 scanning electron

microscope, equipped with electron backscatter diffraction (EBSD), backscattered electron (BSE), and energy dispersive X-ray spectroscopy (EDS) detectors, was used for microstructure characterization.

The heat treated specimens were machined to final geometry (see Figure 1) and polished to remove any surface roughness prior to the uniaxial tensile testing at room temperature according to the ASTM E8 standard [21]. Uniaxial tensile testing was performed at a strain rate of 0.005 mm/mm/min. Due to the travel limit, the extensometer was attached to the specimens during the initial stage of tensile tests up to a strain value of 0.015 (mm/mm) to calculate the yield strength. Upon removal of the extensometer, the tests were continued in force-controlled mode till complete fracture. For all HT conditions, at least three specimens were tested and their average values were reported.

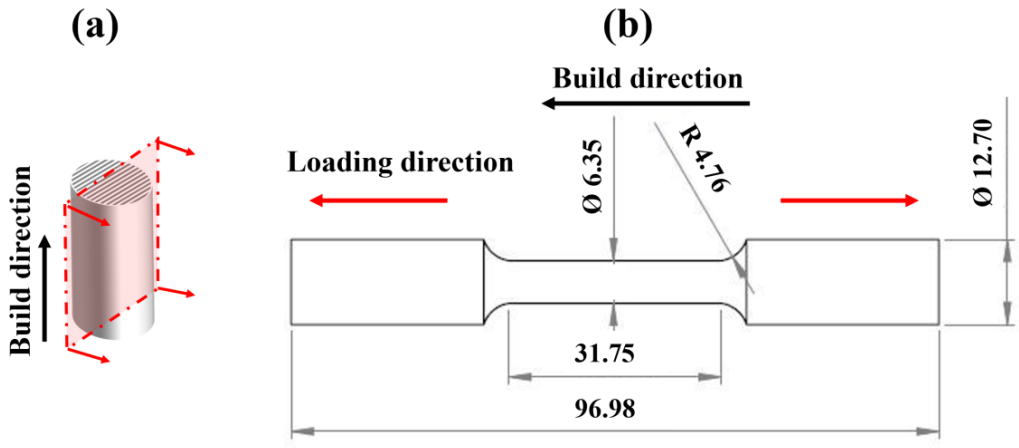

Figure 1. (a) Small coupon for microstructural characterization (plane parallel to the build direction was characterized) and (b) the geometry of the tensile specimens used in this study (Dimensions are in mm).

Results and discussion

BSE micrographs obtained on the transverse plane of the L-PBF and LP-DED fabricated Monel K500 samples are presented in Figure 2 for the NHT and heat treated conditions. The NHT condition showed dendritic microstructure for both L-PBF and LP-DED Monel K500 (see Figure 2(a) & (b)) and elemental micro-segregation (see Figure 3 for LP-DED Monel K500), which are typical for the AMed metallic parts due to high cooling rates during fabrication. Upon full HT, the dendritic microstructure was dissolved into the matrix as solid solution for all HT conditions (see Figure 2(c) - (j)).

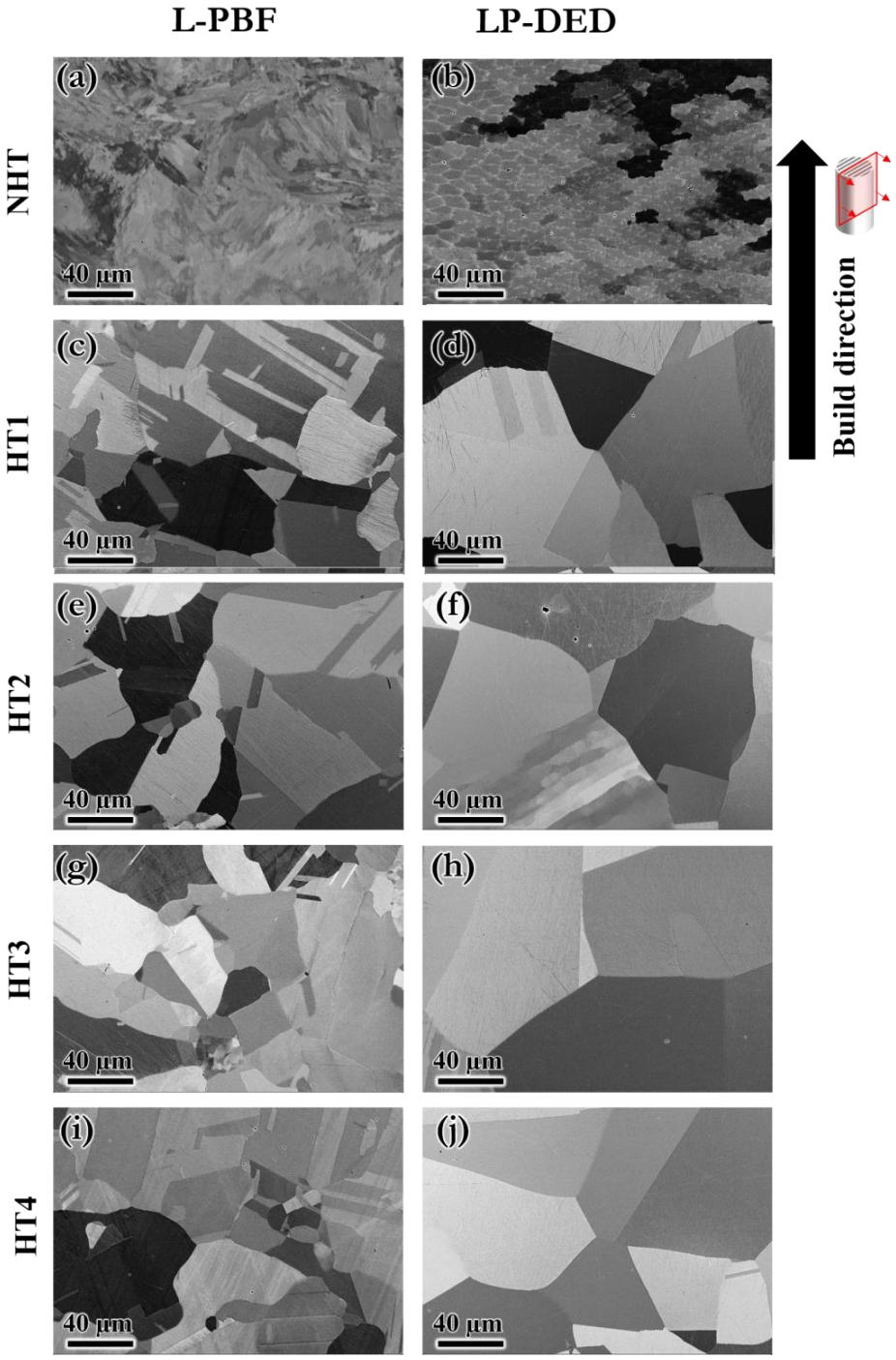

Figure 2. BSE micrographs taken from the transverse plane of L-PBF and LP-DED samples: in (a) & (b) NHT, in (c) & (d) HT1, in (e) & (f) HT2, in (g) & (h) HT3, and in (i) & (j) HT4 conditions. The arrow indicates the build direction.

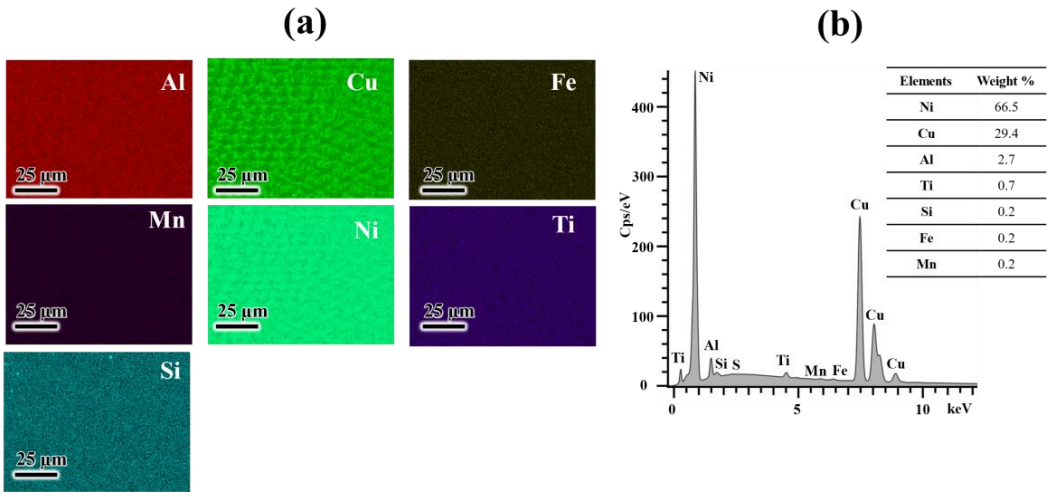

Figure 3. (a) Elemental maps and (b) X-ray spectrum obtained by EDS from the transverse plane of NHT LP-DED Monel K500.

The inverse pole figure (IPF) maps obtained from the EBSD analysis on the transverse plane of the L-PBF and LP-DED samples are presented in Figure 4 for the NHT and heat treated conditions. For NHT and heat treated conditions, the LP-DED samples showed coarser grains compared to the L-PBF ones. In the NHT and heat treated LP-DED samples, the majority of the grains had sizes above 100 µm, while in L-PBF samples, finer microstructure with below 100 µm grain sizes were observed. For all HT conditions, both L-PBF and LP-DED samples exhibited recrystallization and subsequent grain growth with presence of annealing twins in the microstructure (see Figure 4).

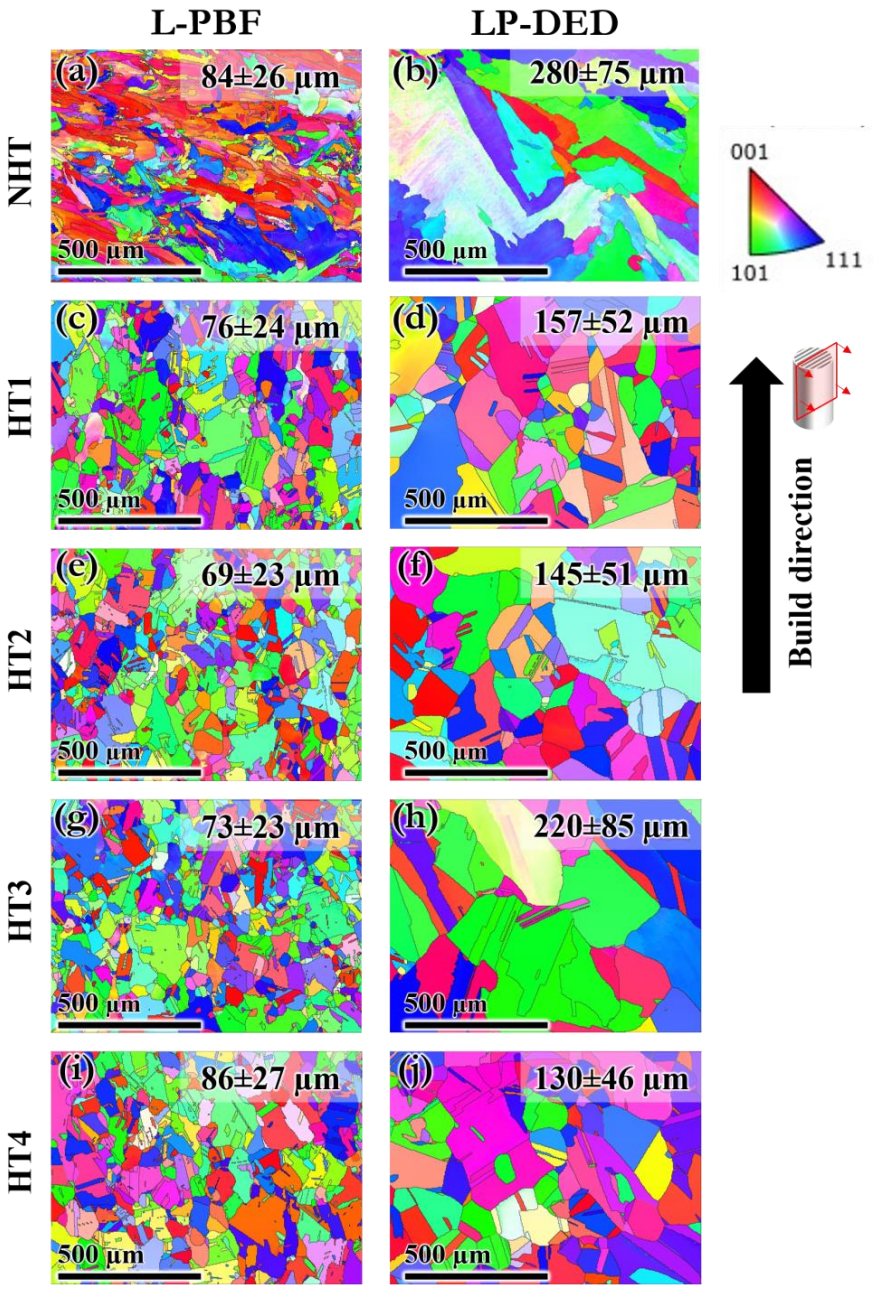

Figure 4. IPF maps taken from the transverse plane of L-PBF and LP-DED samples: in (a) & (b) NHT, in (c) & (d) HT1, in (e) & (f) HT2, in (g) & (h) HT3, and in (i) & (j) HT4 conditions. Material points are colored according to the normal direction of the TD plane. Arrow indicates the build direction.

BSE micrographs obtained from the transverse plane of L-PBF and LP-DED samples are presented in Figure 5 for different HT conditions. The nano-sized γ' precipitates appeared to form in all the HT conditions (see Figure 5). Samples that undergo additional aging steps such as HT3 and HT4, formed coarser γ' precipitates. This is mainly due to longer soaking time during aging, which promotes growth of the precipitates [22,23]. In particular, the size of γ' precipitates in HT4 is larger than those in HT3 due to longer soaking time (6 hr longer) associated with an additional aging step.

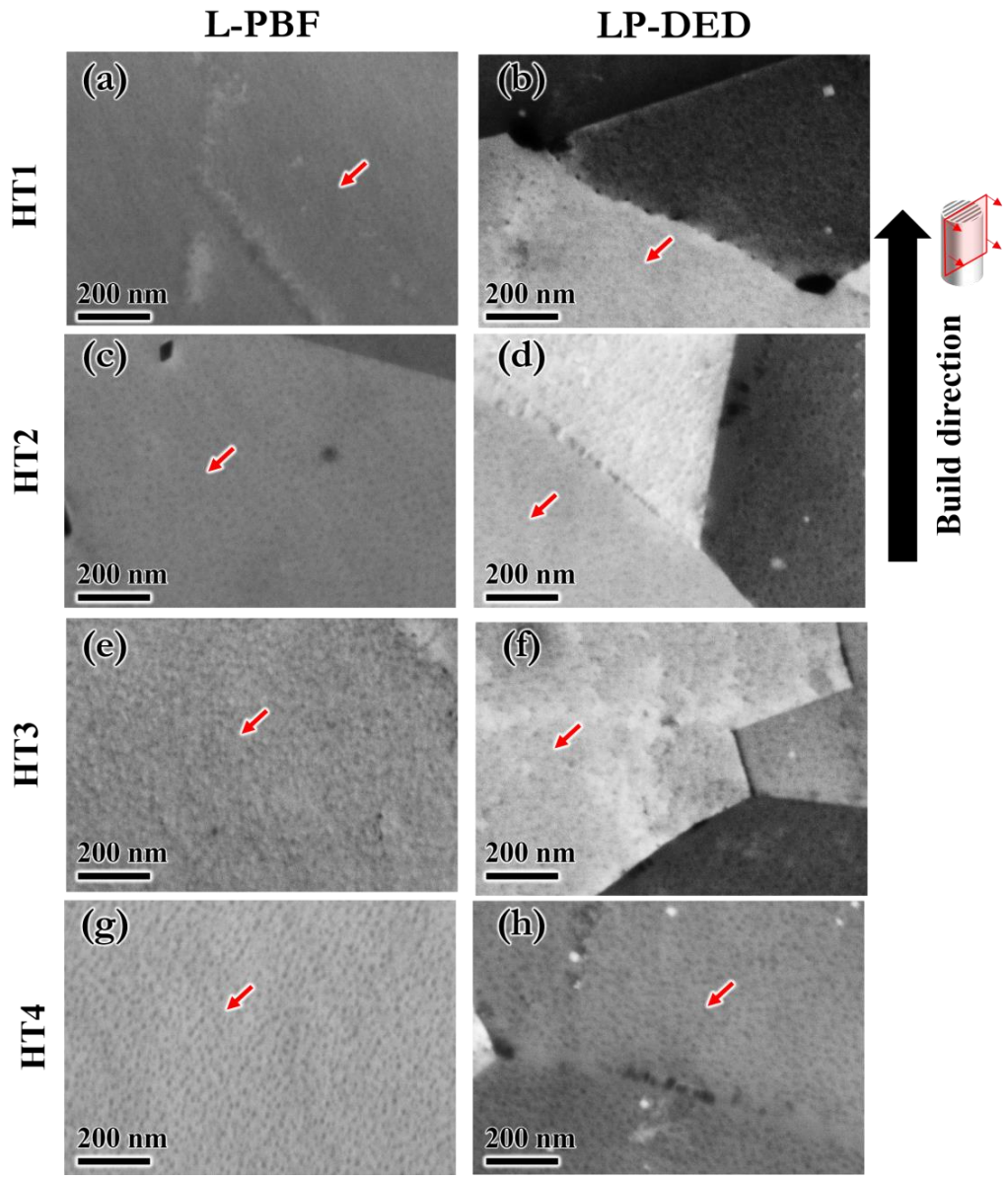

Figure 5. BSE micrographs taken from the transverse plane of L-PBF and LP-DED specimens: in (a) & (b) NHT, in (c) & (d) HT1, in (e) & (f) HT2, in (g) & (h) HT3, and in (i) & (j) HT4 conditions. Red arrowheads point to γ' precipitates. Black arrow indicates the build direction.

Engineering stress-strain curves and the corresponding ultimate tensile strength (UTS), yield strength (YS), and elongation at failure (%EL) for the different heat treated L-PBF and LP-DED fabricated Monel K500 tensile specimens are presented in Figure 6. From HT1 to HT4, increasing trends in YS and UTS were observed for both L-PBF and LP-DED specimens, while decreasing trends were observed for ductility. The highest strength for HT4 could be attributed to larger γ' precipitates at higher volume fractions. For all HT conditions, L-PBF specimens showed higher strength and lower ductility compared to LP-DED counterparts. For instance, HT1 L-PBF Monel K500 specimens showed 37% and 19% higher YS and UTS respectively, and 12% lower %EL than HT1 LP-DED. Higher strength in L-PBF specimens can be attributed to the finer grain structures present in the microstructure compared to LP-DED process (see Figure 4). Among the heat treated L-PBF and LP-DED Monel K500 tensile specimens, HT4 L-PBF Monel K500 exhibited similar tensile properties compared to the wrought Monel K500 alloy [24] (see Figure 6 (b)). To gain deeper insights into the impact of HT, ongoing research is focused on analyzing the fatigue performance of L-PBF and LP-DED Monel K500 alloy.

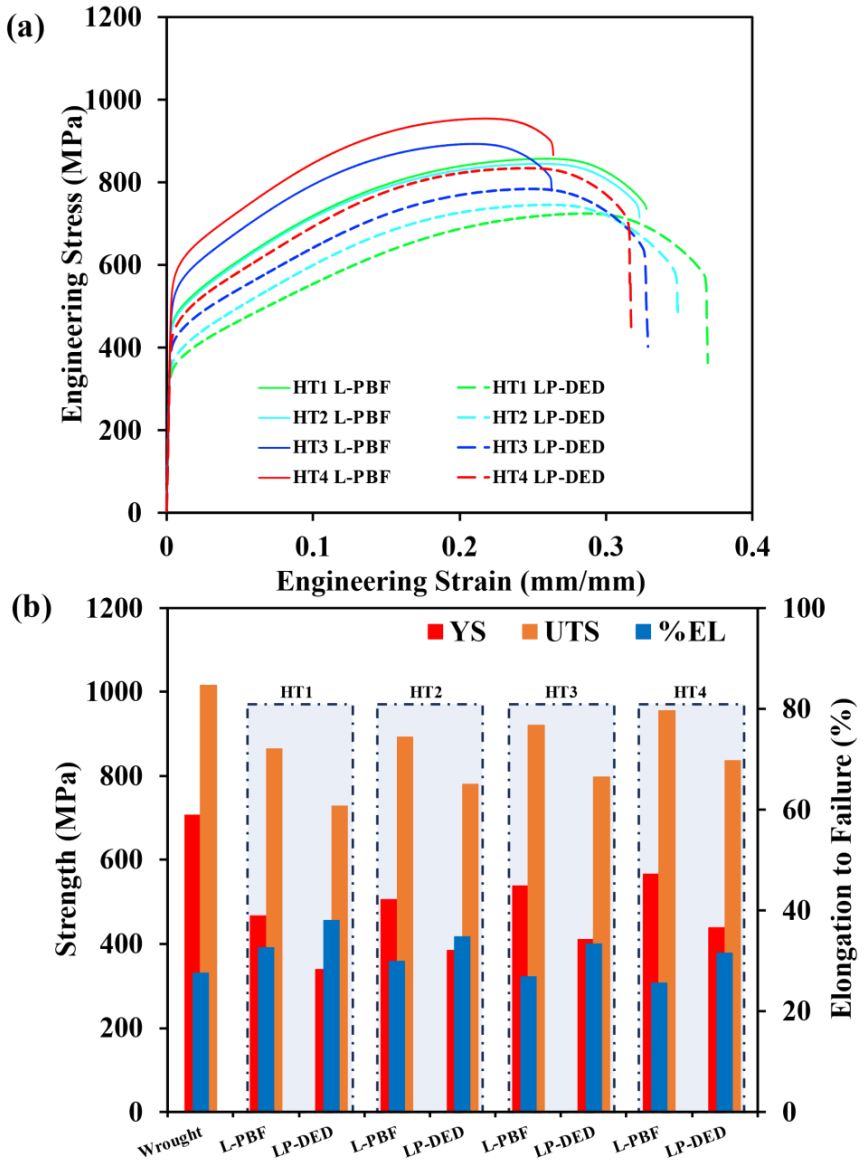

Figure 6. Tensile behavior of HT wrought, L-PBF, and LP-DED Monel K500 (a) Engineering stress-strain curves (b) bar chart showing variations in tensile properties such as UTS, YS, and %EL.

Both L-PBF and LP-DED Monel K500 tensile specimens showed ductile fracture with dimples present on the tensile fracture surfaces (see Figure 7). However, larger sized dimples were observed for the LP-DED specimens compared to L-PBF counterparts. The higher elongation observed in the LP-DED specimens can be attributed to the coarser grain size (see Figure 4). In such cases, the increase in elongation comes at the expense of strength (see Figure 6).

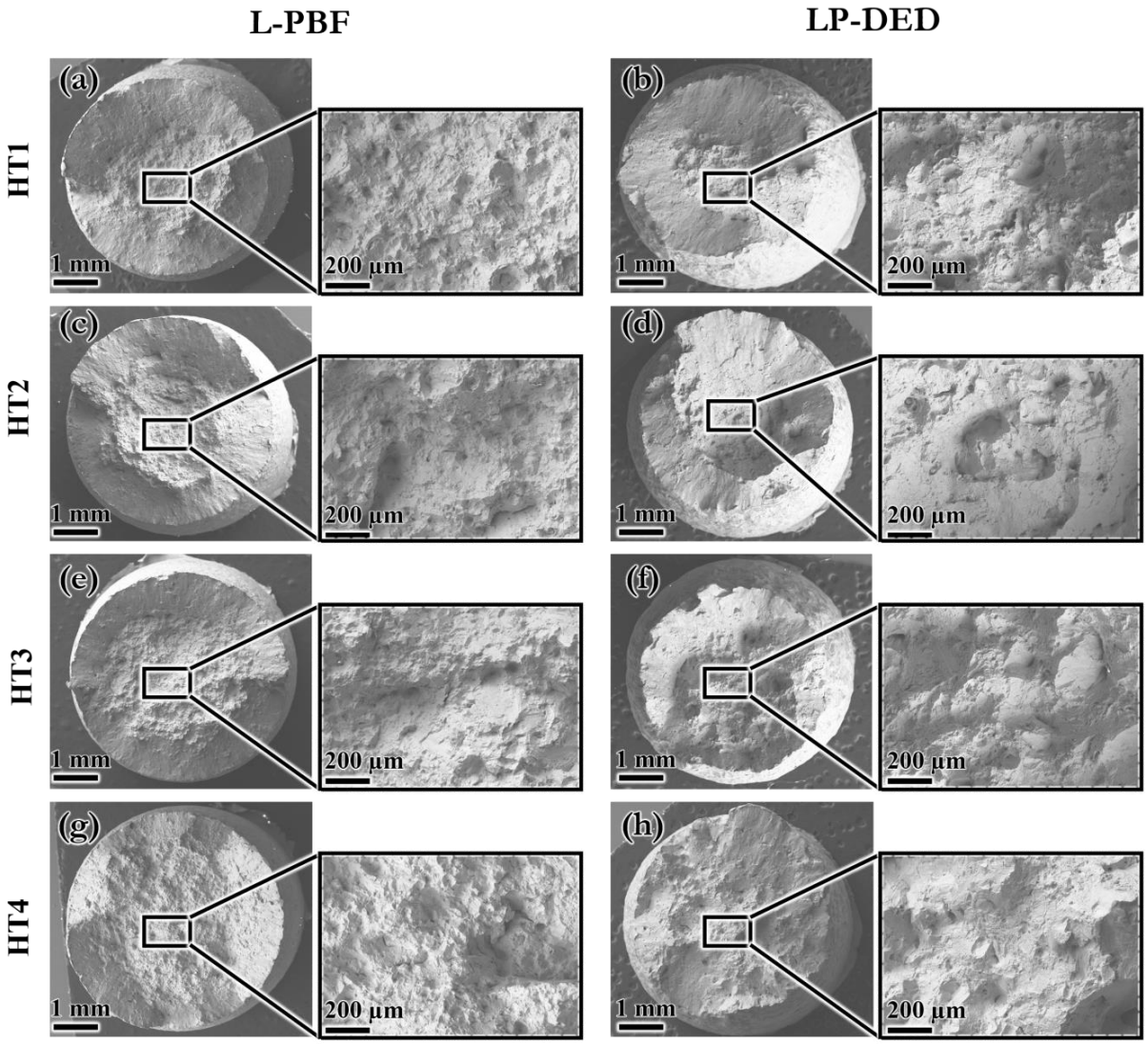

Figure 7. Tensile fracture surfaces of heat treated L-PBF and LP-DED Monel K500 specimens: in (a) & (b) HT1, in (c) & (d) HT2, in (e) & (f) HT3, in (g) & (h) HT4 conditions.

Conclusions

In this study, the effect of different heat treatments (HT) procedures was investigated on the microstructure and tensile properties of laser powder bed fused (L-PBF) and laser powder directed energy deposited (LP-DED) Monel K500. The following conclusions were drawn:

1. Dendritic microstructure was observed for both L-PBF and LP-DED Monel K500 samples in the non-heat treated conditions, which resolved after HT.
2. Heat treated L-PBF samples exhibited finer grain structure compared to LP-DED counterparts.
3. HT condition with longer soaking time during aging showed higher strength in both L-PBF and LP-DED Monel K500, which was ascribed to the growth of the γ' precipitates during aging.
4. L-PBF Monel K500 specimens showed higher strength compared to LP-DED ones, which was ascribed to the finer grain structure.
5. HT4 offered the highest strength for both L-PBF and LP-DED Monel K500 specimens.

Acknowledgment

This study is partially supported by the National Aeronautics and Space Administration (NASA) under Cooperative Agreement No. 80MSFC19C0010. This paper describes objective technical results and analysis. Any subjective views or opinions that might be expressed in the paper do not necessarily represent the views of the NASA or the United States Government.

References

[1] Z. Chen, C. Wang, C. Tang, Y.Z. Lek, S.Y. Kandukuri, H. Du, H. Gao, K. Zhou, Microstructure and mechanical properties of a Monel K-500 alloy fabricated by directed energy deposition, Materials Science and Engineering: A. 857 (2022) 144113. https://doi.org/10.1016/J.MSEA.2022.144113.

[2] O. Marenych, A. Kostryzhev, C. Shen, Z. Pan, H. Li, S. van Duin, Precipitation strengthening in Ni–Cu alloys fabricated using wire arc additive manufacturing technology, Metals (Basel). 9 (2019). https://doi.org/10.3390/met9010105.

[3] A.G. Kostryzhev, O.O. Marenych, Z. Pan, H. Li, S. van Duin, Strengthening mechanisms in Monel K500 alloyed with Al and Ti, J Mater Sci. 58 (2023) 4150–4164. https://doi.org/10.1007/S10853-023-08248-2/FIGURES/8.

[4] Megamex, Monel{®} K-500, (2010) 1–20. http://megamex.com/monel-500-nickel-alloy.htm.

[5] Z. Chen, C. Wang, C. Tang, Y.Z. Lek, S.Y. Kandukuri, H. Du, H. Gao, K. Zhou, Microstructure and mechanical properties of a Monel K-500 alloy fabricated by directed energy deposition, Materials Science and Engineering: A. 857 (2022) 144113. https://doi.org/10.1016/J.MSEA.2022.144113.

[6] A. Kulandaivel, S. Kumar, Effect of magneto rheological minimum quantity lubrication on machinability, wettability and tribological behavior in turning of Monel K500 alloy, Https://Doi.Org/10.1080/10910344.2020.1765179. 24 (2020) 810–836.

[7] U. Esgin, D. Özyürek, H. Kaya, An investigation of wear behaviors of different Monel alloys produced by powder metallurgy, AIP Conf Proc. 1727 (2016) 16. https://doi.org/10.1063/1.4945963/884222.

[8] A. Yadollahi, N. Shamsaei, Additive manufacturing of fatigue resistant materials: Challenges and opportunities, Int J Fatigue. 98 (2017) 14–31. https://doi.org/10.1016/J.IJFATIGUE.2017.01.001.

[9] N. Shamsaei, A. Yadollahi, L. Bian, S.M. Thompson, An overview of Direct Laser Deposition for additive manufacturing; Part II: Mechanical behavior, process parameter optimization and control, Addit Manuf. 8 (2015) 12–35. https://doi.org/10.1016/J.ADDMA.2015.07.002.

[10] P. Gradl, O. Mireles, N. Andrews, Introduction to Additive Manufacturing for Propulsion Systems Additive Manufacture is real …, Propulsion Energy and Forum 2020. (2019).

[11] D. Dev Singh, T. Mahender, A. Raji Reddy, Powder bed fusion process: A brief review, Mater Today Proc. 46 (2021) 350–355. https://doi.org/10.1016/J.MATPR.2020.08.415.

[12] D.G. Ahn, Directed Energy Deposition (DED) Process: State of the Art, International Journal of Precision Engineering and Manufacturing-Green Technology 2021 8:2. 8 (2021) 703–742. https://doi.org/10.1007/S40684-020-00302-7.

[13] M. Muhammad, R. Gusain, S.R. Ghiaasiaan, P.R. Gradl, S. Shao, N. Shamsaei, MICROSTRUCTURE AND MECHANICAL PROPERTIES OF ADDITIVELY MANUFACTURED HAYNES 230: A COMPARATIVE STUDY OF L-PBF VS. LP-DED, (n.d.).

[14] M.M. Rahman, G. Huanes-Alvan, H. Sahasrabudhe, S.K. Chakrapani, Elastic Properties of IN718 Fabricated via Laser Directed Energy Deposition (DED), Proceedings of 2021 48th Annual Review of Progress in Quantitative Nondestructive Evaluation, QNDE 2021. (2022). https://doi.org/10.1115/QNDE2021-74848.

[15] S. Chakraborty, D. Hebert, T.R. Faisal, Variations of In-Plane Mechanical Properties of Cellular Structures With Different Hierarchical Organizations, ASME International Mechanical Engineering Congress and Exposition, Proceedings (IMECE). 12 (2021). https://doi.org/10.1115/IMECE2020-24050.

[16] B. Poudel, H.X. Nguyen, A. Oneil, M.U. Ahmad, Z. Qu, P. Kwon, H. Chung, Selective Laser Melting and Mechanical Properties of Oxide Dispersion Strengthened Haynes 214 Alloy, Proceedings of ASME 2022 17th International Manufacturing Science and Engineering Conference, MSEC 2022. 2 (2022). https://doi.org/10.1115/MSEC2022-85620.

[17] A. du Plessis, I. Yadroitsava, I. Yadroitsev, Effects of defects on mechanical properties in metal additive manufacturing: A review focusing on X-ray tomography insights, Mater Des. 187 (2020) 108385. https://doi.org/10.1016/J.MATDES.2019.108385.

[18] M. Laleh, E. Sadeghi, R.I. Revilla, Q. Chao, N. Haghdadi, A.E. Hughes, W. Xu, I. De Graeve, M. Qian, I. Gibson, M.Y. Tan, Heat treatment for metal additive manufacturing, Prog Mater Sci. 133 (2023) 101051. https://doi.org/10.1016/J.PMATSCI.2022.101051.

[19] Z.D. Harris, J.T. Burns, The effect of isothermal heat treatment on hydrogen environment-assisted cracking susceptibility in Monel K-500, Materials Science and Engineering: A. 764 (2019) 138249. https://doi.org/10.1016/J.MSEA.2019.138249.

[20] E3 Standard Guide for Preparation of Metallographic Specimens, (n.d.). https://www.astm.org/e0003-11r17.html (accessed June 30, 2023).

[21] A.E. Committee, E08, Standard Test Methods for Tension Testing of Metallic Materials, ASTM International, 2020.

[22] G.K. Dey, P. Mukhopadhyay, Precipitation in the Ni-Cu-base alloy monel K-500, Materials Science and Engineering. 84 (1986) 177–189. https://doi.org/10.1016/0025-5416(86)90236-3.

[23] G.K. Dey, R. Tewari, P. Rao, S.L. Wadekar, P. Mukhopadhyay, Precipitation hardening in nickel-copper base alloy monel K 500, Metallurgical Transactions A 1993 24:12. 24 (1993) 2709–2719. https://doi.org/10.1007/BF02659495.

[24] Special Metals - MONEL®, (n.d.). https://www.specialmetals.com/documents/technical-bulletins/monel/.